

On the modelling of cell and lipoprotein transport in the thoracic aorta

Alexander Fuchs^{1,2,*}, Niclas Berg², Lisa Prahl Wittberg²

1. Department of Radiology, Karolinska University Hospital, Stockholm and Department of Medical and Health Sciences, Linköping University, Linköping, Sweden.

2. FLOW & BioMEx, Department of Engineering Mechanics, KTH, 100 44 Stockholm, Sweden.

*Corresponding Author

Email for correspondence: alex@mech.kth.se

Abstract

Purpose: The purpose of the study is to compare and assess modeling of transport cells and lipoproteins by the blood in the human thoracic aorta.

Methods: In the continuum framework, three flux models were considered; Fickian, Zydney-Colton (Z-C) and Leighton-Acrivos (L-A). The transport of spherical particles (cells and lipoprotein of different sizes and densities) under pulsatile flow condition were simulated. The effect of local red blood cell (RBC) concentration (hematocrit) on blood viscosity was considered through Quemada's model. Lagrangian particle transport (LPT) was assessed and compared to the continuum models. Contribution to RBC flux (diffusion) due to gradients in hematocrit, mixture density and viscosity was assessed. Results were extracted in terms of mean and variations in concentrations, residence time and path lengths of RBC and six other cells and lipoproteins.

Results: The effects of local hematocrit variations on the local blood viscosity is large (a factor of more than 2) but the effect on wall shear stress (WSS) indicators is much more modest (few percent). In terms of mean concentration, the three continuum transport models yield local viscosity that deviate by a factor between about 1.3 to 2, as compared to a constant viscosity case. The main contribution to the mass (RBC) flux in the L-A model is from the shear-rate gradient term, followed by the viscosity gradient term and least by the RBC concentration gradient term (low flow rate). The inflow and wall boundary conditions play an important role on the details of the mass transport. The LPT result do converge to the expected concentration at the different outflow boundaries. However, the convergence rate is slow and require more than 30 cardiac periods to get below 2% in outflow hematocrit. Detailed analysis of the RBC paths shows large variations. For the outlet from the thoracic aorta RBC path length and residence time ranging from 0.333 m to 0.0.791 m and from less than one to about four cardiac cycles, respectively. The corresponding values for the LCCA are about 0.2 m to more than 0.5 m and about a quarter to about four cardiac cycles, respectively. The LPT results also show that particles are subject to a lift force driven by strong path curvature and particle to fluid density difference. A simulation with injection of particles in the descending aorta indicated the possibility of upstream transport of particles into the three main arteries branching from the aortic arch.

Conclusions: Continuum transport models depend strongly on calibrated model parameters and the imposed boundary conditions. Counter gradient diffusion may occur as the fluxes are dependent on gradients of shear rate, concentration, and viscosity. LPT has the advantage of accounting for temporal effect and are most appropriate for dilute particle suspensions such as cells (except for RBC) and lipoproteins. LPT though, may require substantially longer computational time when statistical data is sought.

Keywords: Whole blood viscosity, non-Newtonian fluid, Thoracic aorta, LPT, cell and lipoprotein transport.

1. Introduction

Blood as transport medium

As blood is an important carrier of cells and other components (molecules and lipoproteins) the transport of these components depends on local flow conditions, which in turn depend on the rheological properties of blood.

Whole blood experiments revealed the dependence of blood viscosity on red blood cell (RBC) concentration and shear rate (cf Zydney and Colton (1988), Brust et al (2013)). Such experiments were also used to model whole blood viscosity over a wider range of shear rates and hematocrit (cf Quemada et al (1977, 1978) and a recent review by Hund et al (2017)). RBC concentration may vary considerably, but under normal condition it occupies almost half of the total blood volume. With this high level of RBC concentration, RBC phase can be in thermodynamic equilibrium implying that blood may be assumed to behave as a continuum. The continuum assumption implies that the RBCs are considered as one of the phases composing blood. The phase is associated with physical quantities (such as density and viscosity) derived by averaging the RBCs properties over volumes that are small enough to have a meaning in the continuum sense but also large enough to include adequate number of RBCs to have a meaningful average. To account for RBC motion in the continuum framework a transport model must be added. Transport models are often characterized by advection of a substance by the fluid (termed as advection or convection) and a so called “diffusion” component accounting for all other processes causing transport. The literature has a rich number of publications regarding using the advection-diffusion approach both for RBC and other blood components such as white blood cells (WBC), and lipoproteins of different sizes. The expression for the “diffusion” process may be linear (so called “Fickian”) with a constant diffusivity or non-linear with variable diffusivity depending on different parameters, such as fluid, substance concentration and density and mixture viscosity. Most often the gradients of the different parameters are assumed to drive the “diffusion” process. Some examples of modeling of transport of LDL (low density lipoprotein), WBC and RBC are given in the following.

The transport of WBC and VLDL was modeled in the same way as the LDL, by for example Lantz and Karlsson (2012), Liu et al (2009), Hund and Antaki (2009) and Sharifi and Niazmand (2015). As the concentration of these blood components is dilute, one may assume that the interaction within the phase of LDL/VLDL/WBC is little and only hydro-dynamical forces acting on the lipoproteins. Wada and Carino (2004) considered steady-state flow and LDL concentration in an artery with multiple bends. A Fickian diffusivity ($D=5 \cdot 10^{-12} \text{ m}^2/\text{s}$) was assumed. Despite the small value of the diffusivity coefficient the LDL concentration in the near wall region was 35.1% higher than that in the bulk flow. Deng et al (2009) considered the transport of LDL under steady-state condition and the presence of helical motion formed in human aorta. Different boundary conditions were tested along with a constant diffusion coefficient ($D=4.8 \cdot 10^{-12} \text{ m}^2/\text{s}$). The effects of aortic torsion and taper had clear effect on LDL transport, and that adverse correlation between wall shear stress (WSS) and the luminal surface LDL concentration in the aorta. Vijayaratnam et al (2015) considered drug release in stented arteries under steady-state conditions using different rheological models. Drug diffusivity in blood and tissue were set to constant values ($3.89 \times 10^{-11} \text{ m}^2/\text{s}$ and $3.65 \times 10^{-12} \text{ m}^2/\text{s}$, respectively). The choice of different rheological models had clear effect on the length recirculation zone. Nevertheless, the average drug concentration was less affected when using different non-Newtonian models. On the other hand, the spatial distribution of drug in the tissue significantly affected by rheological model. Mpairaktaris et al (2017)

computed steady state flow in a patient-specific aorta and the transport of low-density lipoprotein. The blood viscosity was assumed to obey a power law and in-lumen diffusivity was set to $2.867 \cdot 10^{-11} \text{ m}^2/\text{s}$ and effective diffusivity for the media layer was set to $5 \cdot 10^{-14} \text{ m}^2/\text{s}$. The flux into the wall was assumed to be set to a given value. The conclusion was that the transport of LDL was affected by elevated transmural pressure, leading to near-wall higher LDL concentration. Similar approach was used by Sun et al (2008) for steady-state and pulsatile flows along with transport of LDL and albumin in a coronary artery. Constant diffusivity coefficients for LDL and albumin ($3.5 \cdot 10^{-12}$ and $6.05 \cdot 10^{-12} \text{ m}^2/\text{s}$, respectively) were assumed. Deyranlou et al (2015) considered LDL transport in an axi-symmetric pipe with distensible walls using steady-state convection-diffusion equation with constant diffusivity ($D=2.87 \cdot 10^{-11} \text{ m}^2/\text{s}$ in the blood and lower diffusivity in the tissue).

Iasiello et al (2016) considered LDL transport in the framework of four non-Newtonian models. The convection-diffusion equation was solved for LDL concentration with Kedem-Katchalsky equation combined with porous media relation as boundary condition. The results showed that non-Newtonian effects on mass transport were negligible. Prosia et al (2005) solved the incompressible flow equations with a filtration velocity (Darcy law based) at the wall. The advection-convection equation for LDL transport was solved (two-layer approach) with a linear combination of concentration gradient and filtration velocity-based boundary condition. LDL diffusivity was assumed to be a constant ($8 \cdot 10^{-13} \text{ m}^2/\text{s}$). Liu et al (2011) LDL transport under unsteady flow using non-Newtonian modelling and LDL viscosity based on Stokes-Einstein equation (i.e. $O(10^{-12} \text{ m}^2/\text{s})$). The results showed that in larger part of the aorta, pulsatility of the flow had almost no effect on near wall LDL concentration (about 2% relative to lumen concentration). Hansen and Shadden (2016) studied the near wall transport at high Schmidt number using an own developed analytical expression relating the flow and near-wall mass transport. The advection-diffusion equation employed a constant value ($D=2 \cdot 10^{-10} \text{ m}^2/\text{s}$). Soulis et al (2009) computed LDL transport in the thoracic aorta. A Fickian model diffusivity ($15 \cdot 10^{-12} \text{ m}^2/\text{s}$) was assumed along with a constant infiltration velocity into the wall ($0.6 \cdot 10^{-8} \text{ m/s}$). The main finding was that elevated LDL levels were found near the concave wall and that at peak systole reached 23% higher level than that at inlet to the aorta. Hund and Antaki (2009) proposed an extended convection-diffusion model for handling the transport of platelets and WBC assuming that the concentrations of these blood components is dilute. The model was able to simulate the experimentally observed near-wall increase in platelet concentration. However, the success of the model requires prescribing the RBC concentration distribution.

Souzy et al (2015) studied experimentally the dispersion of dye in the presence of particles. It was found that the diffusion coefficient increases with distance from the wall. The advection-diffusion equation was solved using a linearly varying diffusivity coefficient resulting in quantitative agreement with experiments. In the presence of particles super-diffusive was observed, implying increase of stirring with distance from the wall.

In contrast to the large number of continuum base simulations of lipoprotein transport, Lagrangian Particle Tracking (LPT) approach seems to be popular in one-way interaction (post-processing) for simulating transport of blood components. For example, Arzani (2018) used LPT for determining particle residence times in aneurysmal flows. LPT was also used to compute certain quantities that are associated with individual particles and not the ensemble of particles. Examples of such cases are the platelet activation models of Nobili et al (2008) and that of Soares et al (2013) or the expression for helical flow quantification by Morbiducci et al (2007).

This paper uses the Quemada blood rheology model in the framework of blood mixture continuum equations with the option of modeling transport and non-uniform distribution of the RBCs. LPT is also used for RBC transport, comparing mean quantities with the continuum model. The different rheological model lead to relatively small differences in the local flow conditions. The differences in local flow conditions may manifest in large differences when one considers the (LPT based)

transport of cells and lipoproteins with different physical properties. Hence, the transport of cells (leukocytes, and RBC), lipoproteins (HDL, VLDL; Chylomicrons) and a globular protein that plays a central role in coagulation process (von Willbrand factor, VWF) were also considered.

Material and methods

The geometry of the thoracic aorta was derived from a CT-scan of a healthy patient. The computational domain consists of the ascending aorta, the aortic arch, the descending aorta and the three main branching arteries; the Brachiocephalic Artery (BCA), left Common Carotid Artery (LCCA) and left Subclavian Artery (LSCA)). The blood is assumed to be incompressible with non-constant bulk density which is assumed to depend on the concentration (hematocrit) of Red Blood Cells (RBC). The effect of other blood components was neglected. Thus, the blood is assumed to be a non-homogenous mixture satisfying conservation of mass (Eq. 1a) and momentum (Eq. 1b).

$$\frac{\partial \rho u_i}{\partial t} + \frac{\partial (\rho u_i u_j)}{\partial x_j} = -\frac{\partial p}{\partial x_i} + \frac{\partial}{\partial x_j} \mu \frac{\partial u_i}{\partial x_j} \quad (1a)$$

$$\frac{\partial \rho}{\partial t} + \frac{\partial \rho u_i}{\partial x_i} = 0 \quad (1b)$$

Where ρ , μ are the density and viscosity of the mixture respectively, p is the pressure and u_i is the Cartesian velocity component in the i -direction. The blood is assumed to be non-Newtonian implying that the bulk viscosity depends on the local hematocrit (α) and shear-rate (γ). The simulations herein use the Quemada model [Quemada (1977, 1978)] for accounting for whole blood viscosity. The model is non-linear in terms of the two variables (α and γ), and model parameters. The formulation used herein is as follows:

$$\mu = \mu_p \left(1 - \alpha \frac{k(\gamma, \alpha)}{2} \right)^{-2} \quad (2a)$$

the plasma viscosity $\mu_p = 1.32 \cdot 10^{-3}$ Pa s, γ is the magnitude of the shear-rate tensor $\gamma_{ij} = \frac{1}{2} \left(\frac{\partial u_i}{\partial x_j} + \frac{\partial u_j}{\partial x_i} \right)$ and

$$k(\gamma, \alpha) = \frac{k_0(\alpha) + k_\infty(\alpha) \sqrt{\gamma/\gamma_c(\alpha)}}{1 + \sqrt{\gamma/\gamma_c(\alpha)}} \quad (2b)$$

The parameters γ_c , k_0 and k_∞ are the critical shear rate and non-dimensional intrinsic viscosities related to low and high shear rates, respectively. The formulation of equation (2b) used here are those of Cokelet (1987). The coefficients $k_0(\alpha)$, $k_\infty(\alpha)$ and $\gamma_c(\alpha)$ are given by

$$k_0 = e^{3.874 - 1041\alpha + 13.8\alpha^2 - 6.738\alpha^3} \quad (2c)$$

$$k_\infty = e^{1.3435 - 2.803\alpha + 2.711\alpha^2 - 0.6479\alpha^3} \quad (2d)$$

$$\gamma_c(\alpha) = e^{-6.1508 + 27.923\alpha - 25.6\alpha^2 + 3.679\alpha^3} \quad (2e)$$

The RBC concentration (α) is assumed to be governed by an advection-diffusion equation:

$$\frac{\partial \alpha}{\partial t} + u_i \frac{\partial \alpha}{\partial x_i} = \frac{\partial}{\partial x_i} j_i(\alpha) \quad (3)$$

The main challenge of this formulation is defining the flux of α . Three models were used in the following. These are the models due to Fickian, Zydney and Colton (1988) (Z-C) and Leighton and Acrivos (1987) (L-A).

The simplest possible model is to express the diffuse flux as being Fickian.

$$j_i = D_b \frac{\partial \alpha}{\partial x_i} \quad (3a)$$

With D_b the transport diffusivity. The value of D_b is a constant, commonly associated with the Stokes-Einstein relation of the order of $D_b = 10^{-12}$ m²/s. Based on experimental data Casa and Ku

(2017), based on Zydney and Colton (1988), state that $D_b=10^{-8}$ m²/s. Further cases were by us computed using also smaller values of diffusivity constants: $D_b=10^{-7}$ (not shown here) and $D_b=10^{-6}$ m²/s.

Zydney and Colton (1988) expressed the flux depending also on the concentration gradient, based on the diffusivity of deformable particle suspension:

$$j = [D_b + K_\alpha \alpha a^2 \gamma (1 - \alpha)^n] \nabla \alpha \quad (3b)$$

Where the shear-rate, $\gamma = \sqrt{2S_{ij}S_{ij}}$ being the norm of the shear-rate and a being the mean of the RBC radius, D_b the Brownian diffusivity, K_α and n are model parameters. The following parameter values were used in the simulation herein: $D_b=10^{-8}$; $a=410^{-6}$; $K_\alpha=0.15$; $n=0.8$.

A generalization of the above model may be derived if one assumes that diffusion may be driven by forces due to inhomogeneity in different parameters of the mixture. Based on scaling arguments Leighton and Acrivos (1987), Phillips et al. (1992) propose a model of the following form:

$$j_i = (D_b + K_\alpha \alpha a^2 \gamma) \frac{\partial \alpha}{\partial x_i} + K_\gamma \alpha^2 a^2 \frac{\partial \gamma}{\partial x_i} + K_\mu \alpha^2 a^2 \gamma \frac{1}{\mu} \frac{\partial \mu}{\partial x_i} \quad (3c)$$

The model parameters are K_α , K_γ and K_μ are non-dimensional constants, which determine the contribution of the gradients in hematocrit, shear-rate, and viscosity to the flux, respectively. The following parameter values were used in the simulation herein: $D_b=10^{-8}$; $a=410^{-6}$; $K_\alpha=0.43$; $K_\gamma=0.43$; $K_\mu=0.65$.

The boundary conditions for solving the flow (equations (1a) and (1b)) were a time-dependent inlet flowrate, as the used by Fuchs et al (2019). At the four outlets the flow rates were given as portion of the inlet flow rate (Benim et al (2011)): BCA 15%, LCCA and LSCA 7.5% each and at the outlet from the descending aorta 70%. In all the computed cases, unless explicitly stated otherwise, the boundary conditions for equation (3) were as follows: Inlet RBC concentration was a smoothed top-hat function $\alpha=A_0(1-\tanh((|\zeta-\zeta_0|)/\varepsilon))/2$, where ε regulates the thickness of the shear-layer and A_0 (=0.45) is the centerline hematocrit and $|\zeta-\zeta_0|$ is the distance from the wall. A constant value of $\alpha=0.25$ was set on the walls and zero gradient at the outlets. The details of the methods for solving equations (1) and (2) was given in Fuchs et al (2019).

The results below were computed using the Quemada rheology model (equation (2)) along with one of three RBC transport models (equations (3a), (3b) and (3c), respectively). Table 1 shows the computed cases along with the parameters that were used for the simulation.

Table 1: Transport models and their parameters used in the simulations

Case	HR / CO	Transport model	Model parameters
C1	75 BPM/6 LPM	Fickian eq (3a)	$D_b = 0.91 \cdot 10^{-8}$
C2	75 BPM/6 LPM	Fickian eq(3a)	$D_b = 0.91 \cdot 10^{-6}$
C3	75 BPM/6 LPM	Zydney & Colton (Z-C) eq (3b)	$D_b = 0.91 \cdot 10^{-8}$; $a = 4 \cdot 10^{-4}$ $k = 0.08$; $n = 0.8$
C4	75 BPM/6 LPM	Leighton & Acrivos (L-A) eq (3c)	$a = 4 \cdot 10^{-4}$; $K_\alpha = 0.43$; $K_\gamma = 0.43$ $K_\mu = 0.65$; $D_b = 10^{-8}$

The flux model described above assume continuum, with the underlying assumption of thermodynamic equilibrium with the RBC phase. The assumption seems to be reasonable due to the high-volume fraction of the RBC. The continuum assumption is less reasonable for other cells or

lipoproteins. The alternative is to use a Lagrangian particle tracking (LPT) approach in which the particles are tracked given the forces that act on the particle assuming a one-way interaction. In the simulations herein, only the viscous drag was considered. In the post-processing step also the size and location of the buoyancy lift-force (F_c) was assessed from the following relation:

$$F_c = \kappa u_t^2 (\rho_p - \rho_b) V_p \quad (4)$$

where u_t , κ , ρ_p , ρ_b and V_p are the particle velocity tangential to its path, the path curvature, particle and fluid density and particle volume, respectively.

The computed flow fields were used to compute the motion of RBC, WBC, platelets, three lipoproteins and vWF. The lipoproteins were HDL, VLDL, Chylomicrons. The data related lipoproteins can be found in Chaudhary et al (2019) and Upadhyay (2018). Cell densities follow data by Norouzi et al (2017). The particles were released intermittently at the inlet at random position at a given rate. In the following we use “particles” for cells, lipoproteins, and macromolecules. The physical properties of these seven solid spherical “particles” are given in Table 2:

Table 2: Dimension sizes (μm) and densities (g/l) of the “particles” used in the simulations

	RBC	WBC	Platelet	HDL	VLDL	Chylomicrons	vWF
Diameter (μm)	8	20	2	0.02	0.1	2	1
Density (g/L)	1125	1080	1075	1200	950	900	1102

Particle were released at the inlet to the thoracic aorta continuously, intermittently or a bolus under a given period of time. The particles had zero velocity at the inlet plane were injected at random location with a specified rate. The boundary conditions for the particle at solid walls was fully elastic rebound (i.e. the wall normal velocity component changes sign at the wall while maintaining the wall parallel velocity components). The particles are tracked until the leave the computational domain at one of the four exits (BCA, LCCA, LSCA, and the inlet to the abdominal aorta).

Results

Continuum models

The results in the following are related to the cases in Table 2.

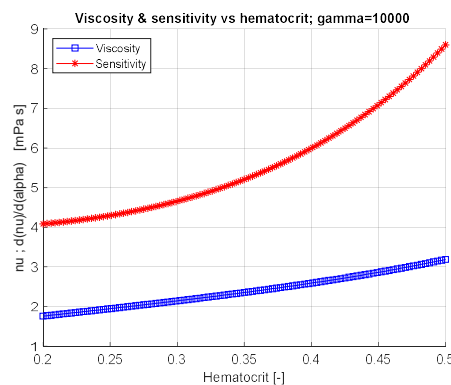


Figure 1: Quemada rheology model: Viscosity vs hematocrit for a shear-rate or 1000 s^{-1} . The sensitivity (i.e. the derivative of viscosity with respect to hematocrit) shows a monotone increase in sensitivity with the hematocrit.

In the Quemada model the viscosity depends on the shear-rate and the local RBC concentration. Fig 1 depicts the behavior of the Quemada model for a given shear-rate (1000 s^{-1}) over a hematocrit

range between 0.2 and 0.5. The figure also depicts the sensitivity of the viscosity to changes in hematocrit. For the lower range, the sensitivity is lower (3% increase due to 1% increase in hematocrit) and at the end of the range the sensitivity increases by a factor larger than 10 (i.e. 35%).

Since the viscosity model is rather sensitive to hematocrit (and also to shear-rate), the changes in the viscosity in the simulation using the three transport model for RBC (equations (3a)-(3c)) were assessed. The impact of the models on the viscosity was measured through the two following parameters (Johnston et al (2004)).

$$I_L = \frac{\mu}{\mu_{ref}} ; \quad I_g = \frac{1}{N} \frac{[\sum_{i=1}^N (\mu(x,t) - \mu_{ref})^2]^{1/2}}{\mu_{ref}} \quad (5)$$

The I_L parameter measure the relative increase in (space) mean kinematic viscosity over a reference value (taken to be 3.310^{-6}). The I_g parameter measures the root mean square (rms) fluctuation around the reference value, μ_{ref} . Fig 2 depicts the two parameters I_L and I_g during a cardiac cycle for a case of HR=75 BPM and CO=6 LPM. Two Fickian cases were simulated; one using a diffusion coefficient ($D_b=0.91 \cdot 10^{-8} \text{ m}^2/\text{s}$) and the second (“Fickian*100”) with D_b hundred times larger than the former. In these simulations the hematocrit was kept constant at $\alpha=0.45$. The other two cases use a non-uniform inlet α distribution, scaled during the cardiac cycle in proportion with the volumetric flow rate. At the wall, a fixed value $\alpha=0.25$ was used. As noted, the (space) averaged viscosity is largest (about twice as large as the reference value) when the hematocrit is kept at a fixed value of 0.45. The viscosity decreases during systole mainly due to the increase in shear-rate (shear-thinning fluid and model) and increases during diastole. This behavior is common to all four cases in the figure. The deviation from the reference value are roughly similar for the three models (increasing the Fickian diffusion coefficient by a factor of 100, the Z-C and the L-A models). The temporal response follows the cardiac cycle as the original Fickian model. The level of relative spatial fluctuations (I_g) are large when compared to the relative level of viscosity itself. I_g is

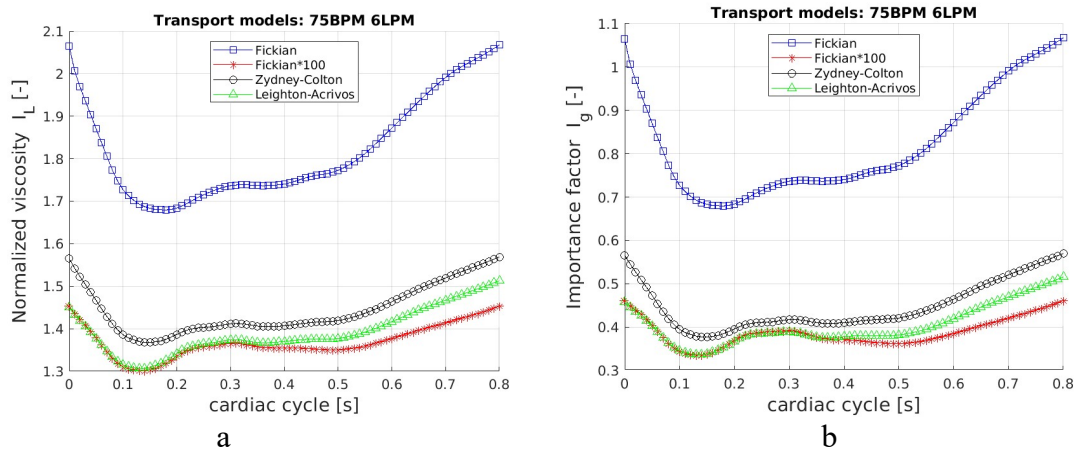


Figure 2: **a.** The variation of the viscosity (relative to the reference value, I_L). **b.** The rms of the spatial variation of viscosity relative to the reference value, normalized with the reference viscosity (I_g). The definition of the two parameters I_L and I_g are given in equation (5).

Viscosity plays an important role in forming the wall shear-stress. Arterial wall pathologies were related to metrics of WSS, temporal variation of WSS or WSS indicators such as TAWSS, OSI and RRT. Arzani and Shadden (2016) review the history of using and applying these parameters in simulations of blood flow. The sensitivity of these parameters to transport models of RBC and thereby on whole blood viscosity is given in Table 3a and 3b for the peak and mean values of common WSS indicators. The impact of the viscosity on WSS indicators follow the behavior of the viscosity. The Fickian model (with $D_b = 0.91 \cdot 10^{-8}$) results on largest viscosity and WSS parameter

values. The differences between the other models (Cases C2 to C4) are much smaller (a few percent). This behavior is valid both for peak values as for the mean values.

Table 3a: Peak values of WSS indicators using different transport RBC models

Case/Transport model	WSS	dWSS/dt	TAWSS	OSI	RRT
C1 - Fickian $D_b = 0.91 \cdot 10^{-8}$	428.89	39243	13.9	0.4956	0.870
C2 - Fickian $D_b = 0.91 \cdot 10^{-6}$	349.27	33223	13.8	0.4974	0.632
C3 – Zydney – Colton	330.07	44157	14.0	0.4972	0.806
C4 – Leighton - Acrivos	324.26	35100	13.9	0.4987	1.053

Table 3a: Mean values of WSS indicators using different transport RBC models

Case/Transport model	WSS	dWSS/dt	TAWSS	OSI	RRT
C1 - Fickian $D_b = 0.91 \cdot 10^{-8}$	1.28	21.05	1.606	0.025	0.00015
C2 - Fickian $D_b = 0.91 \cdot 10^{-6}$	1.25	17.86	1.533	0.025	0.00009
C3 – Zydney – Colton	1.33	18.44	1.734	0.025	0.00008
C4 – Leighton - Acrivos	1.28	18.44	1.580	0.025	0.00008

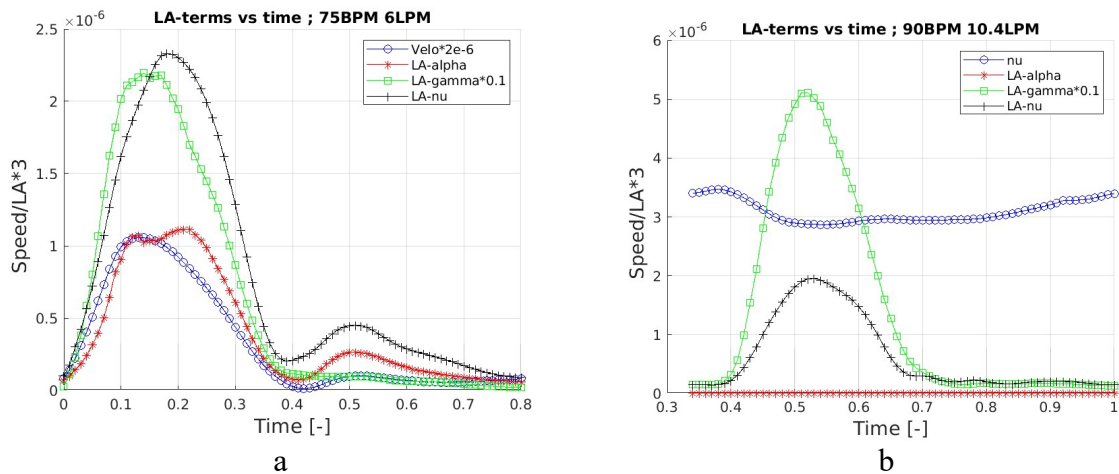


Figure 3: The contribution of each of the three terms to the RBC flux vs the cardiac cycle (normalized time). The left frame includes the scaled velocity inlet velocity to enable assessment of the temporal behavior. The right frame includes the corresponding viscosity behavior.

The contribution of different mechanism to the flux (equation (3)) was studied computing explicitly each of the terms in the Leighton-Acrivos model. Figure 3 depicts the contribution to the RBC flux, by the different terms on the right hand side of equation (3c). The largest contribution is from viscosity gradient. This contribution is roughly larger (at peak systole) by an order of magnitude as compared to the next largest one due shear rate gradient. The commonly used concentration gradient has the smallest contribution in systole. In diastole the contribution of shear-rate gradient diminishes faster than the other two terms making the concentration gradient almost as large as the

contribution from viscosity gradient. With increasing HR and CO (right frame in Fig 3), the shear-rate in systole dominates and simultaneously the viscosity effect decreases.

LPT transport of RBC

As the RCB concentration is high the continuum model assumption is reasonable. Using LPT approach is also possible but requires accounting for different forces that act on each of the RBC. These forces include hydrodynamical drag and lift forces, forces due to density differences between RBC and the carrier fluid, and not least interaction force between the RBCs themselves. For other blood components, i.e. other cells than RBC, lipoproteins and macromolecules, the concentration is low with large distance (relative to particle size) between the particles, leading to the lack of thermodynamical equilibrium within the particle phase. The LPT simulations here in are simpler in the sense that only drag is accounted for in a one-way coupling mode. Other particle properties such as residence time, path length and lift force due to path curvature and density were assessed using the simulated flow data.

The results in the following were derived by injecting intermittently RBC with a frequency of 1 Hz, with injection during 0.5 s and no injection during the second half of the period (Fig 4). The injection continued for up to 50 cardiac periods. Other simulation used both continuous injection and intermittent injection with lower frequency with the aim of studying wash-out effects.

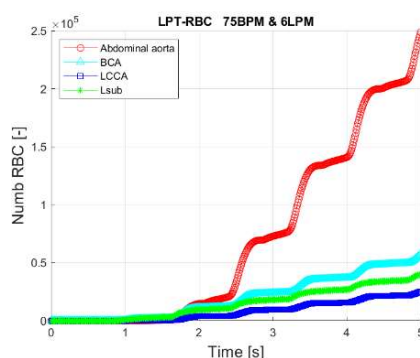
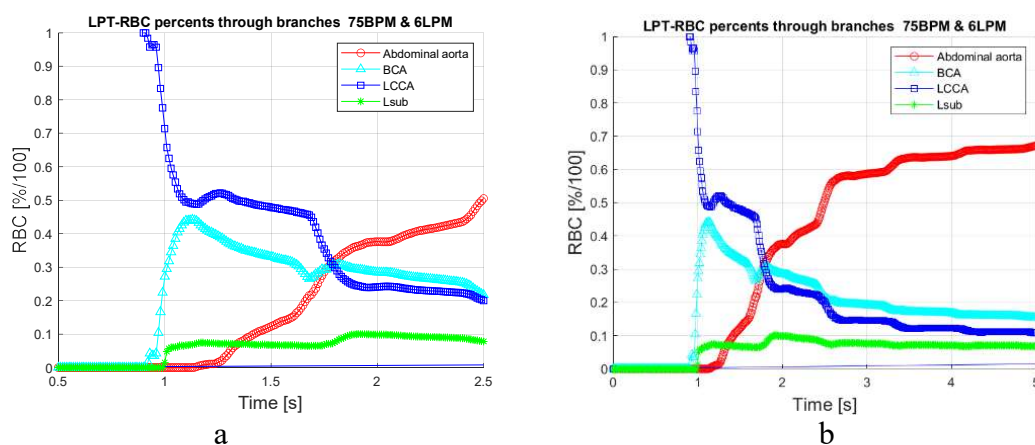


Figure 4: Number of RBCs leaving different parts of the aorta and main branching arteries. The effect of the intermittent injection is clearly observed in the concentration with increasing slope (0.5 s duration and 1 s cycles).



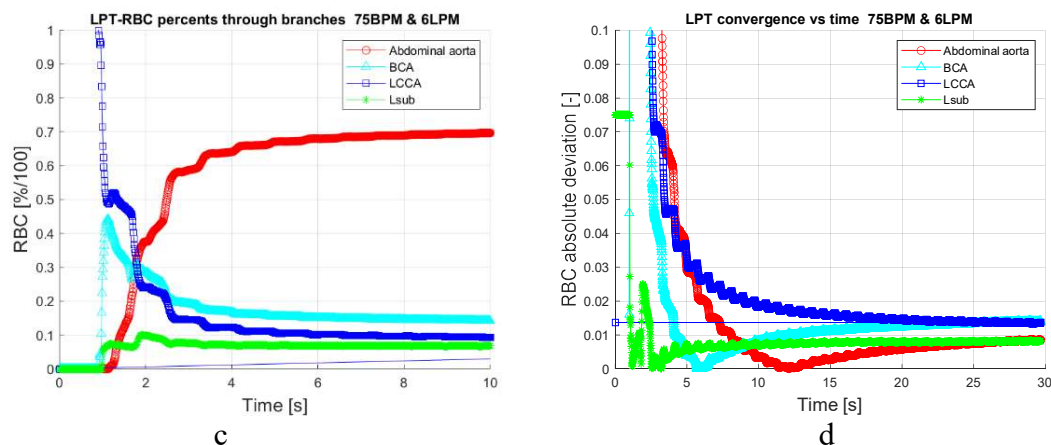
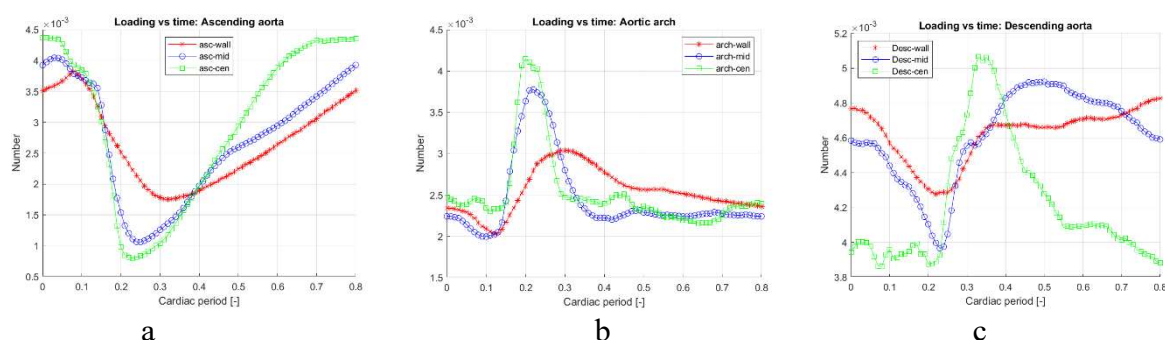


Figure 5: Temporal development of RBC concentration at the different outlet branches. Frames a-c depict the relative concentration (defined the number of particles leaving the branch relative to the total number leaving the thoracic aorta). Frame d depicts the asymptotic deviation from the reference value with a hematocrit of $\alpha=0.45$ and specified flow rates in each of the branches.

Transport of light particles (Chylomicrons)

Distribution of Chylomicrons (“particles”) in the thoracic aorta was assessed by dividing the aorta into ten segments in the “axial” direction and 10 segments in the “radial” direction. The Chylomicrons in the sections was averaged into three axial groups (denoted as ascending, arch and descending) and three radial groups (near-wall, mid and central). Fig 6 depict the portion of particles relative to total number) as function of the cardiac cycle. The number of particles varies most in the ascending segment during the deceleration phase of systole, increasing during early systole and diastole. The opposite behavior is observed in the arch, with largest concentration at peak deceleration during systole. In the descending aortic segment, the concentration is lower in the central segment but increases during end systole and early diastole. Fig 7 compares the particle concentration in the three radial segments along the aorta. Fig 7 show that the concentration of Chylomicrons is largest and slowly varying in the near wall region. The impact of retrograde flow is most clear near the ascending aorta, leading to a sharp reduction of particles in all segments of the ascending aorta. A corresponding increase in concentration is observed in the aortic arch.



Figures 6: Chylomicrons relative numbers in the ascending (a), arch (b) and descending (c) segments, divided into the near-wall, middle and central regions as function of cardiac cycle.

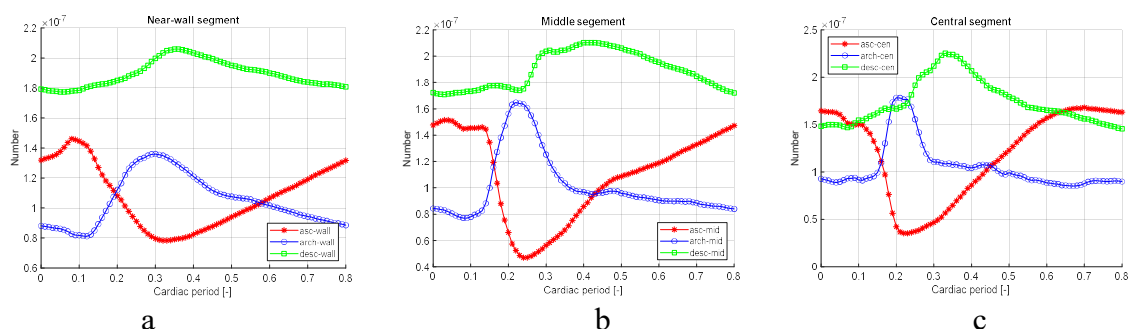
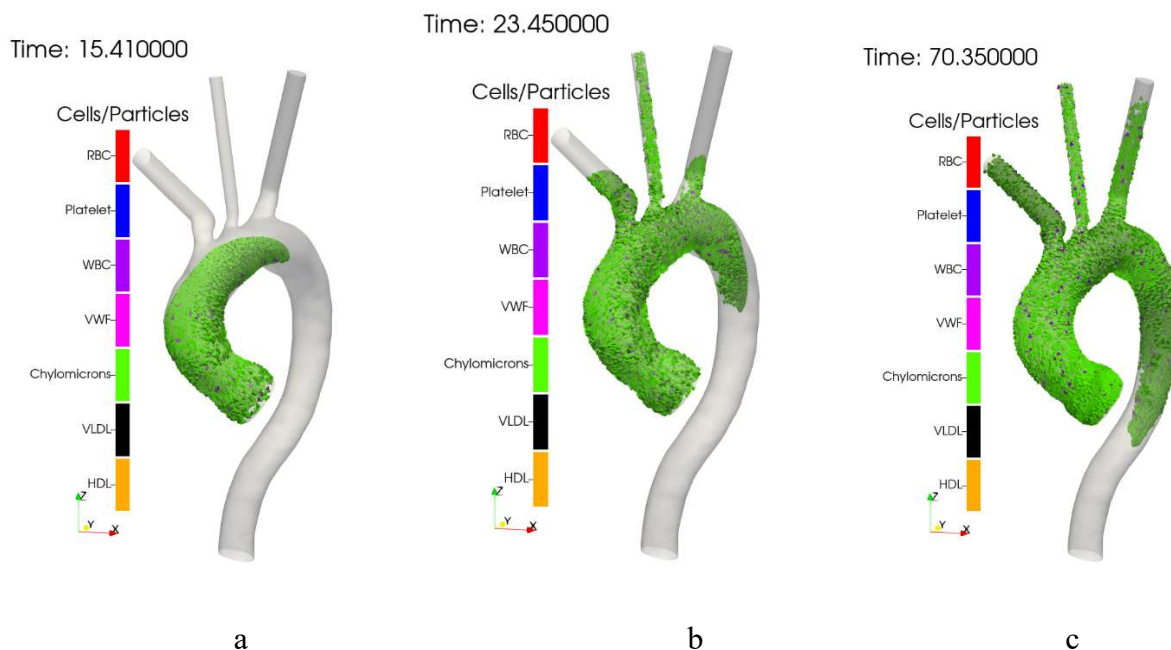
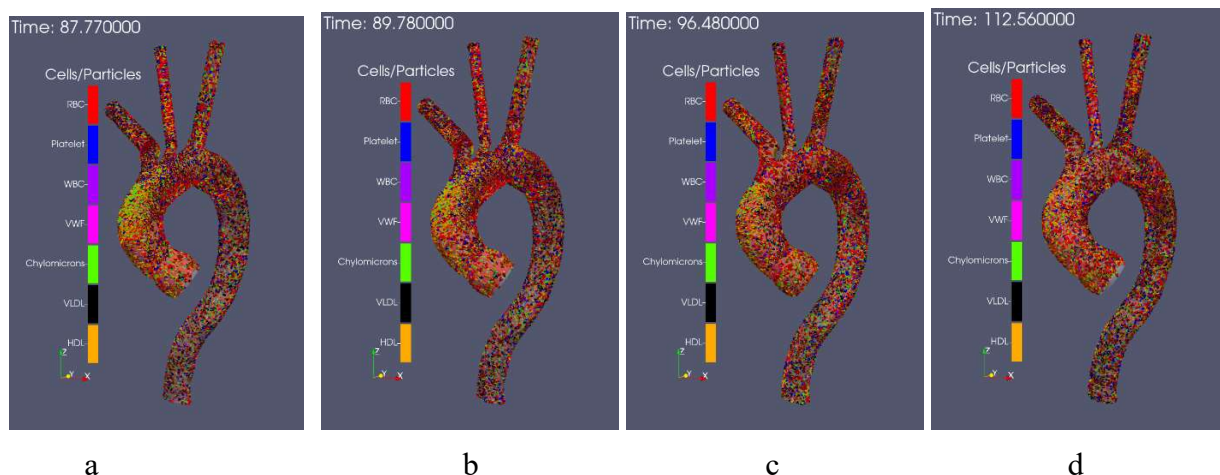


Figure 7: Chylomicrons relative numbers in the near-wall region (a); mid-segment (b) and central segment (c) of the aorta.

In addition to the effects of rheological models on the wall parameters and larger flow structures, the impact of blood rheology on the transport of the species listed in Table 2 was considered. Figure 8 depicts three instantaneous pictures of the distribution of two “particles” (Chylomicrons and platelets) in the aorta. The three frames are related to different time instances in the cardiac cycle. In the initial stages the near-wall region is dominated by Chylomicrons (green) with more platelets are visible at later times in the aortic arch (8b) and the proximal part of the descending aorta (8c). The figure also shows the higher flow in the inner bend of the aorta as compared to the outer one. The transport into the arteries branching from the aorta is uneven. LCCA is the first to be filled followed by BCA and LSCA. The figure shows qualitatively that the relative number of platelets in BCA seems to be larger than in LCCA.



Figures 8: Instantaneous distribution of Chylomicrons and platelets (both with the same size of 2 μm but differ in density) during three time instances during the cardiac cycles.



Figures 9: Instantaneous distribution of the seven “particles” at different time instances during the cardiac cycle. Note the variations in concentrations in the different frames.

Table 4a: (Newtonian model)

Particle-Type	Aortic outlet	BCA-outlet	LCCA-outlet	LSCA-outlet
HDL	0.711826861	0.147037208	7.22004250E-02	6.89355135E-02
VLDL	0.711745143	0.147068366	7.22368658E-02	6.89496323E-02
VWF	0.711800218	0.147101507	7.21339211E-02	6.89643547E-02
Chylomicron	0.711734831	0.147180423	7.22394064E-02	6.88453168E-02
Platelet	0.711838782	0.147051618	7.23103955E-02	6.87991902E-02
RBC	0.711672544	0.147240952	7.24097565E-02	6.86767176E-02
WBC	0.711507559	0.147243142	7.23936111E-02	6.88557103E-02

Table 4b: (Quemada with Leighton-Acrivos)

Particle-Type	Aortic outlet	BCA-outlet	LCCA-outlet	LSCA-outlet
HDL	0.662720084	0.165377498	9.37514827E-02	7.81509504E-02
VLDL	0.667746305	0.160863593	9.43337008E-02	7.70564005E-02
VWF	0.667453647	0.161007702	9.43328440E-02	7.72058144E-02
Chylomicron	0.667517185	0.160908714	9.43330154E-02	7.72411004E-02
Platelet	0.667398751	0.161084965	9.42773372E-02	7.72389323E-02
RBC	0.662227750	0.165355176	9.40300301E-02	7.83870369E-02
WBC	0.667492092	0.160861194	9.48849842E-02	7.67617077E-02

When all seven particles (altogether over 1 million) are tracked, the instantaneous picture becomes less clear, as depicted in Fig 9. Nevertheless, one may observe that non-homogenous particle distribution in each of the frames, with shift in concentration along the aorta and at different parts of the cardiac cycle. To quantify the differences among the transport of different particles and rheological models the averages of the particle concentration at the four outlets are considered. Tables 4 show the accumulated portion of particles leaving each of the exits from the aorta, namely the BC, LC, LSCA and the inlet to the abdominal aorta (i.e. outlet from the thoracic aorta). Table 4a and 4b correspond to the Newtonian-Fickian and the Quemada-Leighton-Acrivos models, respectively. The blood distribution in all cases was set to a fixed proportion of the inlet flow rate

to 0.15, 0.075, 0.075 and 0.70, respectively. In contrast to these figures, the portion of the different particles in the different branches is close to each other but differs from that of the specified flow rates through the branches. These simulations were relatively short and were limited to 5 cardiac cycles. As seen in Tables 4 the different particles outlet values are closest to the specified flow rates in the Newtonian case (about 1.6%). For that model, also the differences between the particles is small. As noted from Fig 5 for statistically converged data more cardiac cycles are required.

Table 5: Residence time (age, Tables 5a-5d) and path lengths (Tables 5e-5h) of RBC and Chylomicrons at the four outlets. For cases the arithmetic mean, root mean square (rms), maximal and minimal values are specified. Table 5a-5d and 5e-5h correspond to cases C1 to C4, respectively. The cases are specified in Table 1.

C1	RBC - age				Chylomicron - age			
	mean	rms	max	min	mean	rms	max	min
LCCA	1.16831	0.373423	6.98003	0.736206	1.18028	0.406082	6.95231	0.736206
LSCA	1.85175	0.772796	7.24194	0.909292	1.83947	0.763135	7.30002	0.909292
BCA	1.54689	0.600646	7.27571	0.816269	1.55187	0.620446	7.48572	0.816269
Outlet	2.11269	0.625344	7.75305	1.03638	2.11187	0.625871	7.84789	1.036383

C2	RBC - age				Chylomicron - age			
	mean	rms	max	min	mean	rms	max	min
LCCA	1.2251	0.38174	4.57002	0.726568	1.21942	0.439445	6.68936	0.726282
LSCA	1.81553	0.567319	4.93071	0.913094	1.80628	0.688412	7.15342	0.911038
BCA	1.5629	0.508177	4.82968	0.813648	1.55222	0.581016	7.37000	0.819034
Outlet	2.13997	0.529732	4.98352	1.04675	2.15659	0.646544	7.58093	1.050533

C3	RBC - age				Chylomicron - age			
	mean	rms	max	min	mean	rms	max	min
LCCA	1.20732	0.412255	7.34058	0.748043	1.20152	0.392161	6.81628	0.748043
LSCA	1.79197	0.688595	7.23241	0.920458	1.79341	0.684155	7.32665	0.920458
BCA	1.55737	0.621444	7.67058	0.801038	1.55411	0.604007	7.86545	0.801038
Outlet	2.14246	0.622052	7.41021	1.07033	2.14447	0.623656	7.41024	1.07033

C4	RBC - age				Chylomicron - age			
	mean	rms	max	min	mean	rms	max	min
LCCA	1.21562	0.423111	7.31283	0.721111	1.21491	0.412763	6.00012	0.721111
LSCA	1.82197	0.683783	7.07006	0.916203	1.82026	0.680264	7.16461	0.916203
BCA	1.57286	0.619572	7.60001	0.813504	1.57482	0.618847	7.31918	0.813504
Outlet	2.14448	0.625831	7.46152	1.03622	2.14483	0.627753	7.62023	1.03622

C1	RBC - path-length			Chylomicron - path-length		
	mean	rms	max	mean	rms	max
LCCA	0.104073	0.072336	0.22986	0.103971	0.0722841	0.2298588
LSCA	0.066742	0.034296	0.17867	0.066840	0.0343446	0.1786451
BCA	0.077930	0.043127	0.22436	0.077919	0.0430542	0.2264542
Outlet	0.113563	0.063911	0.26590	0.113554	0.0639487	0.2658811

C2	RBC - path-length			Chylomicron - path-length		
	mean	rms	max	mean	rms	max
LCCA	0.144314	0.074012	0.303087	0.110264	0.067665	0.231112
LSCA	0.093165	0.052794	0.261301	0.072292	0.035040	0.177694
BCA	0.121119	0.070897	0.254755	0.084297	0.043403	0.221993
Outlet	0.156055	0.080545	0.311049	0.114012	0.062449	0.269622

C3	RBC - path-length			Chylomicron - path-length		
	mean	rms	max	mean	rms	Max
LCCA	0.107103	0.067438	0.232953	0.107515	0.067513	0.232672
LSCA	0.070328	0.033685	0.173564	0.069787	0.033929	0.174566
BCA	0.083887	0.045475	0.233117	0.083733	0.045689	0.233125
Outlet	0.113899	0.063549	0.270968	0.114063	0.063601	0.270846

C4	RBC - path-length			Chylomicron - path-length		
	mean	rms	max	mean	rms	max
LCCA	0.111960	0.067551	0.230073	0.111844	0.0675106	0.230064
LSCA	0.069824	0.034270	0.184075	0.069935	0.0343919	0.184063
BCA	0.082790	0.043674	0.219839	0.083022	0.0437195	0.223661
Outlet	0.113770	0.062488	0.270727	0.113714	0.0624057	0.269066

Table 5 show information not captured by the averaged mass flux through the boundaries. The residence time and path lengths of the RBC and Chylomicrons the individual particles have different histories. The ratio of maximal and minimal residence time is about seven to ten for the descending aorta and the LCCA outlets, respectively. There are much less pronounced differences (about 1% residence time for LSCA) between RBC and Chylomicrons. The rms values are large as compared to the mean and maximal values, indicating the spread in particle histories. The impact of the transport models (C1-C4) in terms of the maximum the residence time is significant when it comes to C1 as compared to the other three (C2, C3 and C4). The differences are less pronounced in terms of mean, rms and minimal residence times. In terms path-length for RBC, Case C2 differs most (by up to about 40%) from the others, whereas the maximal path-length of the Chylomicrons differences are much smaller (less than 2%).

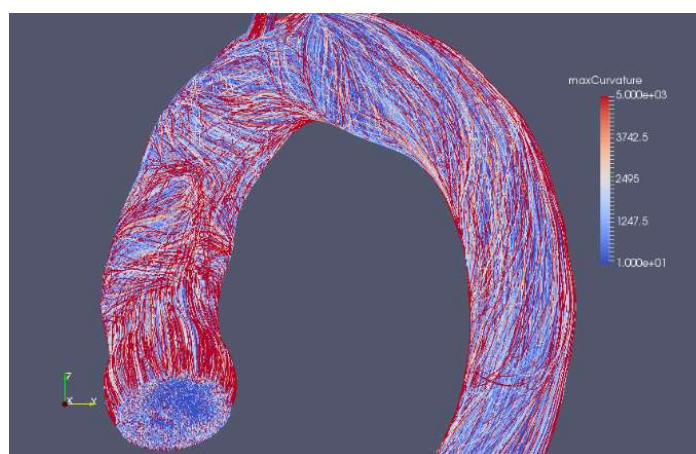


Figure 10: Particle paths colored with curvature. The curvature range is up to 5000 m^{-1} implying that the smallest radius of curvature in the flow was down to 0.2 mm.

In the LPT simulation only drag was accounted for. For particles with densities that differ strongly from that of the blood mixture, centrifugal force may be significant. To assess this aspect the radius of curvature of the particle paths was computed for case C1. Fig 10 depicts particle path lines colored by their path curvature. It was noted that the smallest radius of curvature was as small as 0.2 mm.

A clinically interesting application for particle transport was the question whether particles could be transported from descending aorta into the main arteries branching from the aortic arch. Spherical particles with a diameter of 50 μm and density of 1125 kg/m^3 were released randomly in a plane at end-systole. The particles (5500 in number) were released in a plane about 3 cm downstream of the distal part of the LSCA. The particles were released with zero velocity and were followed over 3 cardiac cycles. Figure 11 depict the particle paths colored by particle residence time (age). As seen, the particles not only were transport upstream in the aorta but during this period some of them (about 6%) ended up in the subclavian artery. Particles with different sizes and densities were also evaluated and it was found that particles could reach, not only LSCA but also into both BCA and LCCA.

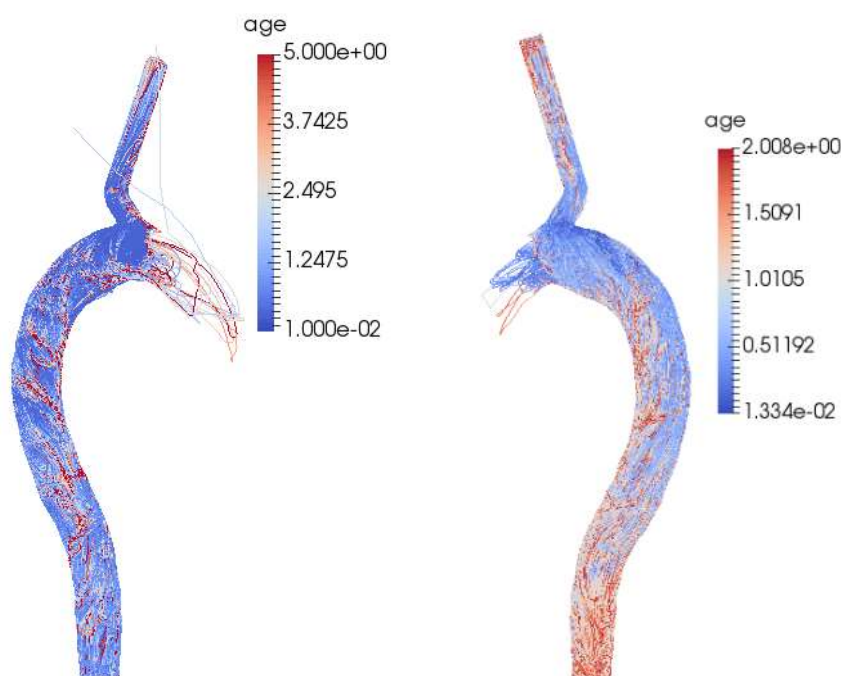


Figure 11: Particle paths colored by particle age. The particles were released about 3 cm downstream of the branching of the subclavian artery during different times during the cardiac cycle. The particles had the same size and density as RBC and were released with 0 velocity and the end of systole. The color bars indicate a resolution up to 5 s (left frame) and up to 2 s (right frame), respectively. Heart rate 90 BPM at 10 LPM. About 6% of the inserted particles were washed out from the subclavian artery.

Discussion

In the framework of continuum modeling, the impact of using different models for the fluxes of TBC was considered. Two of the models were of Fickian type (i.e. gradient diffusion with constant diffusion coefficient) as well as two flux models based on gradients of particle concentration (Zydney and Colton) and a second model that includes also contribution from gradients of shear rate and viscosity (Leighton and Acrivos).

When the impact of the transport models is compared in terms of viscosity level over the cardiac cycle, a clear difference is noted between the Fickian case (C1) with diffusivity coefficient of 10^{-8} m^2/s , as suggested by Casa and Ku (2017) and Zydney and Colton (1988) and a second one (C2) with a diffusivity coefficient of 10^{-6} m^2/s . This value for the effective diffusivity is much smaller than the one that can be derived from Stokes-Einstein relation; namely order of 10^{-12} m^2/s as was also used in the studies presented in the introduction. The explanation for this discrepancy given by Casa and Ku (2017) was that the enhanced diffusivity is the result of enhanced mixing caused by particle rotation and shear-induced collisions. This view is shared also by Omori et al (2013) who found using numerical simulations that shear-induced RBC diffusion was significantly anisotropic with larger component in the velocity gradient direction as compared to that in the vorticity direction. The spanwise component was larger by a factor of more than 5 compared to the other spanwise component. The fact that further increase in the effective transport diffusivity to 10^{-6} m^2/s (case C2) results in fluid viscosity close to the gradient based models (Z-C and L-A) (Fig 2). The rationale in the increase in the transport diffusivity was that fluid viscosity reflects momentum transfer and the low particle Stokes number, implies that the particle follows closely the fluid, resulting in particle diffusivity close to that of fluid viscosity. It should be noted that the diffusivity models and corresponding model parameters were developed under steady-state conditions. For externally imposed oscillations Shapiro and Brenner (1990) found that with increasing oscillation period the axial dispersivity was significantly reduced.

The study of the contribution of the different terms to the particle flux gives some further insight into the diffusivity of the transport process. As shown in Fig 3a during systole the shear rate gradient contribution dominates over the fluid viscosity gradient term which in turn is larger than the commonly used concentration gradient. In diastole the shear rate is low and its contribution to particle transport viscosity is low. At higher heart- and flow- rate (Fig 3b) the shear rate contribution is largest followed by more than an order of magnitude smaller viscosity gradient contribution. The different gradient may counter act each other leading to so called *counter-gradient diffusion* for one or two of the terms in the L-A model. An example for such situation is at locations with non-vanishing shear-rate. Due to the shear-thinning property of blood the gradient of viscosity would have opposite sign to that of the shear gradient and the total flux is determined by largest of these two contradicting fluxes.

The comparison between the continuum models for RBC and the corresponding LPT approach shows that the average concentration at the four outlets are in good agreement with each other (within 1-2%). However, the LPT convergence rate may require large number of cardiac cycles if the level of required accuracy of the average is below a few percent. The LPT approach is, however, most natural for other dilute blood components due to difficulties related to the contributions and calibration of the effective transport diffusivity. The transport of Chylomicrons in the thoracic aorta was studied in terms of “axial” (along the aorta) and “radial” segments. The results show substantial variation in space along the aorta (Fig 6) and in the radial direction (Fig 7). The largest concentration of the lighter than RBC Chylomicrons was largest near the wall though no explicit model was used to enforce flux into the wall as is commonly done with the continuum models.

The results also show that the differences between the transport of particles of different sizes is not sensitive to mean quantities at the outlets (Tables 4a and 4b) when using the same fluid viscosity model. However, there is a clear difference between the results when different models are used. The differences are due to the (rather small) differences in the flow and viscosity fields. The only force acting on the particles is the (Stokes) drag force which includes the effect of local fluid viscosity. This effect is averaged out over large number of particles leading to similar values of outlet concentrations for the different particles. However, individual particles may have very different histories as shown in Table 5, expressed in terms of particle residence time and particle path lengths. The table shows that mean values may differ considerably from peak and rms values. Thus,

when the properties of individual particles are important (such as in the case of platelet activation) it is important to keep track of individual particles. Continuum models are by nature express only (space) averaged values.

Another particle property which is individual is related to the forces acting on the particle. For particles with density that differs considerably from that of the fluid mixture, the lift force associated with path curvature may be important. As shown in Fig 10 the smallest radius of curvature in the thoracic aorta case was as low as 0.2 mm. An estimate of the lift force due to curvature (equation 4) is of the order of 10^{-10} N, which is the same order as that of Stokes drag.

Upstream particle transport from the descending aorta into arteries branching from the aortic arch was found to correlate well with the findings of Wehrum et al (2015) who used 2D transesophageal echocardiography to investigate flow reversal in the descending aorta. Patients with strong retrograde flow had higher risk for developing cerebral embolism. Retrograde transport particles of different size and density particles into the vessels leading the brain should be therefore further explored.

The main limitations in the continuum studies herein are related to using rigid wall and the impact of the assumption on probably overestimating retrograde flow near the wall. The wall boundary conditions for the continuum model did not include in-wall flux models. The corresponding LPT wall condition was limited to simple particle rebound condition. For the RBC case the one-way interaction is too coarse and should be assessed better with a two-way or four-way coupling approach.

References:

- Agarwal R, Sarkar A, Paul S, and Chakraborty S - A portable rotating disc as blood rheometer. *Biomicrofluidics* 13, 064120 (2019); doi: 10.1063/1.5128937
- Arzani A, Shadden SC. Characterizations and Correlations of Wall Shear Stress in Aneurysmal Flow. *J Biomech Eng.* 2016;138(1):0145031-01450310. doi:10.1115/1.4032056
- Arzani A. 2018 Accounting for residence-time in blood rheology models: do we really need non-Newtonian blood flow modelling in large arteries? *J. R. Soc. Interface* **15**: 20180486. <http://dx.doi.org/10.1098/rsif.2018.0486>
- Benim AC, A. Nahavandi, A. Assmann, D. Schubert, P. Feindt, S.H. Suh - Simulation of blood flow in human aorta with emphasis on outlet boundary conditions. *Applied Mathematical Modelling* 35 (2011) 3175–3188
- Brust, M. & Schaefer, C. & Pan, L. & Garcia, Mike & Arratia, Paulo & Wagner, C.. (2013). Rheology of Human Blood Plasma: Viscoelastic Versus Newtonian Behavior. *Physical Review Letters*. 110. 078305. 10.1103/PhysRevLett.110.078305.
- Casa LDC and Ku DN - Thrombus Formation at High Shear Rate. *Annu. Rev. Biomed. Eng.* 2017. 19:415–33 <https://doi.org/10.1146/annurev-bioeng-071516-044539>
- Casson, N. 1959 Rheology of disperse systems. Pergamon Press, London.
- Chaudhary J, Bower J and Corbin IR - Lipoprotein Drug Delivery Vehicles for Cancer: Rationale and Reason. *Int. J. Mol. Sci.* 2019, 20, 6327; doi:10.3390/ijms20246327 www.mdpi.com/journal/ijms
- Cokelet, G. 1987 The rheology and tube flow of blood. *Handbook of Bioengineering* p. 14.
- De Nisco G, Zhang P, Calò K, Liu X, Ponzini R, Bignardi C, Rizzo G, Deng X, Gallo D and Morbiducci U, - What is needed to make low-density lipoprotein transport in human aorta computational models suitable to explore links to atherosclerosis? Impact of initial and inflow boundary conditions. *J Biomech* 68 (2018) 33–42. <https://doi.org/10.1016/j.jbiomech.2017.12.009>

- Deng, X., X. Liu, D. Li, F. Pu, S. Li, and Y. Fan. A numerical study on the flow of blood and the transport of LDL in the human aorta: the physiological significance of the helical flow in the aortic arch. *Am. J. Physiol. Circ. Physiol.* 297:163–170, 2009.
- Fuchs, A. & Berg, N. & Prah Wittberg, L. (2019). Stenosis Indicators Applied to Patient-Specific Renal Arteries without and with Stenosis. *Fluids*. 4.26. DOI:10.3390/fluids4010026.
- Hund SJ, Antaki JF. An extended convection diffusion model for red blood cell-enhanced transport of thrombocytes and leukocytes. *Phys Med Biol.* 2009;54(20):6415–6435. doi:10.1088/0031-9155/54/20/024
- Hund SJ, Kameneva MV and Antaki JF - A Quasi-Mechanistic Mathematical Representation for Blood Viscosity. *Fluids* **2017**, **2**, 10; doi:10.3390/fluids2010010
- Iasiello M, Vafai K, Andreozzi A, and Bianco N - Analysis of non-Newtonian effects on Low-Density Lipoprotein accumulation in an artery. *J Biomech* **49** (2016) 1437–1446.
<http://dx.doi.org/10.1016/j.jbiomech.2016.03.017>
- Jordan A, David T, Homer-Vanniakam S, Graham A and Walker P. - The effects of margination and red cell augmented platelet diffusivity on platelet adhesion in complex flow. *Biorheology*, 2004;41(5):641-53.
- Lantz L and Karlsson M -Large eddy simulation of LDL surface concentration in a subject specific human aorta. *J Biomech* 45 (2012) 537–542 <https://doi.org/10.1016/j.jbiomech.2011.11.039>
- Leighton D and Acrivos A - The shear-induced migration of particles in concentrated suspensions. *J. Fluid Mech.* (1987), vol. 181, pp 415-439
- Liu X, Fan Y, Deng X, Zha F - Effect of non-Newtonian and pulsatile blood flow on mass transport in the human aorta. *J Biomech* **44** (2011) 1123–1131
- Liu X, Pu F, Fan Y, Deng X, Li D, Li S. - A numerical study on the flow of blood and the transport of LDL in the human aorta: the physiological significance of the helical flow in the aortic arch. *Am J Physiol Heart Circ Physiol* **297**: H163–H170, 2009; doi:10.1152/ajpheart.00266.2009
- Morbiducci U, Ponzini R, Grigionid M, Redaelli A - Helical flow as fluid dynamic signature for atherogenesis risk in aortocoronary bypass. A numeric study. *J Biomech* **40** (2007) 519–534
- Mpairaktaris DG, Soulis JV, and Giannoglou –GD, - Low density lipoprotein transport through patient-specific thoracic arterial wall *Computers in Biology and Medicine*, **89**, 2017, Pages 115-126.
<https://doi.org/10.1016/j.compbimed.2017.07.025>
- Nobili, M., Sheriff, J., Morbiducci, U., Redaelli, A. and Bluestein, D. Platelet activation due to hemodynamic shear stresses: damage accumulation model and comparison to in vitro measurements. *ASAIO J* 54, 64-72 (2008).
- Norouzi N, Bhakta HC, Grover WH (2017) - Sorting cells by their density. *PLoS ONE* 12(7): e0180520.
<https://doi.org/10.1371/journal.pone.0180520>
- of Rheology 16, 99{127.
- Omori T, Ishikawa T, Imai Y and Yamaguchi T - Shear-induced diffusion of red blood cells in a semi-dilute suspension. *J. Fluid Mech.* (2013), vol. 724, pp. 154_174. doi:10.1017/jfm.2013.159
- Phillips RJ, Armstrong RC, Brown RA, Graham AL, and Abbott JR - A constitutive equation for concentrated suspensions that accounts for shear induced particle migration. *Physics of Fluids A: Fluid Dynamics* 4, 30 (1992); doi: 10.1063/1.858498
- Prosia M, Zunino P, Perktold K, Quarteroni A – Mathematical and numerical models for transfer of low-density lipoproteins through the arterial walls: a new methodology for the model set up with applications to the study of disturbed luminal flow. *J Biomech* **38** (2005) 903–917. doi:10.1016/j.jbiomech.2004.04.024
- Quemada, D. 1977 Rheology of concentrated disperse systems and minimum energy dissipation principle. *Rheologica Acta* 16 (1), 82{94.
- Quemada, D. 1978 Rheology of concentrated disperse systems ii. a model for non-newtonian shear viscosity in steady ows. *Rheologica Acta* 17 (6), 632-642.

- Shapiro M, and Brenner H, - Taylor dispersion in the presence of time-periodic convection phenomena. Part II. Transport of transversely oscillating Brownian particles in a plane Poiseuille flow. *Physics of Fluids A: Fluid Dynamics* **2**, 1744 (1990); doi: 10.1063/1.857701
- Sharifi A, Niazmand H - Analysis of flow and LDL concentration polarization in siphon of internal carotid artery: Non-Newtonian effects *Computers in Biology and Medicine* **65** (2015), 93-102.
- Soares JS, Sheriff J and Bluestein D - A novel mathematical model of activation and sensitization of platelets subjected to dynamic stress histories. *Biomech Model Mechanobiol* **12**, 1127-41 (2013).
- Soulis J, Giannoglou G, Dimitrakopoulou M, Papaioannou V, Logothetides S and Mikhailidis D - Influence of Oscillating Flow on LDL Transport and Wall Shear Stress in the Normal Aortic Arch. *The Open Cardiovascular Medicine Journal*, 2009, **3**, 128-142 **DOI: [10.2174/1874192400903010128](https://doi.org/10.2174/1874192400903010128)**
- Souzy M, Yin X, Villermaux E, Abid C, Metzger B - Super-diffusion in sheared suspensions. *Phys Fluids*, 2015, **27** (4), pp.41705 ff10.1063/1.4918613ff. fihal-01449403f
- Sun N, Torii R, Wood NB, Hughes AD, Thom SA, Xu X. Computational Modeling of LDL and Albumin Transport in an In Vivo CT Image-Based *JBioech46_TransportThoracicAorta.pdf* Human Right Coronary Artery. *ASME. J Biomech Eng.* 2008;131(2):021003-021003-9. doi:10.1115/1.3005161.
- Upadhyay RK - Lipoproteins as drug delivery vehicles for cancer and tumor therapeutics. *J Stem Cell Res Ther.* 2018;4(3):53–63.
- van Wyk S, Wittberg, LP, Bulusu KV, Fuchs L, Plesniak MW - Non-Newtonian perspectives on pulsatile blood-analog flows in a 180 degrees curved artery model. *Phys Fluids*, **27**(7), 071901, 2015. DOI: 10.1063/1.4923311
- Vijayaratnam PR, O'Brien CC, Reizes JA, Barber TJ, Edelman ER. The Impact of Blood Rheology on Drug Transport in Stented Arteries: Steady Simulations. *PLoS One.* 2015;**10**(6):e0128178. Published 2015 Jun 12. doi:10.1371/journal.pone.0128178
- Wada S, Karino T. Theoretical prediction of low-density lipoproteins concentration at the luminal surface of an artery with a multiple bend. *Ann Biomed Eng* **30**: 778–791, 2002.
- Wu WT, Aubry N, Massoudi M and Antaki JF - Transport of platelets induced by red blood cells based on mixture theory. *International Journal of Engineering Science* **118** (2017) 16–27
- Wu WT, Aubry N, Massoudi M, Kim J and Antaki JF - A numerical study of blood flow using mixture theory. *International Journal of Engineering Science* **76** (2014) 56–72 , <http://dx.doi.org/10.1016/j.ijengsci.2013.12.001> .
- Wu WT, Yang F, Antaki JF, Aubry N, Massoudi M. Study of blood flow in several benchmark micro-channels using a two-fluid approach. *Int J Eng Sci.* 2015;95:49–59. doi:10.1016/j.ijengsci.2015.06.004
- Zydney A. and Colton CK (1988). Augmented solute transport in the shear flow of a concentrated suspension. *PCH. Physicochemical hydrodynamics*, **10**(1), 77-96.
- Zydney, AL, Oliver JD and Colton CK, - A constitutive equation for the viscosity of stored red cell suspensions: Effect of hematocrit, shear rate, and suspending phase. *J Rheology*, 1991, **35**(8), pp.1639-1680